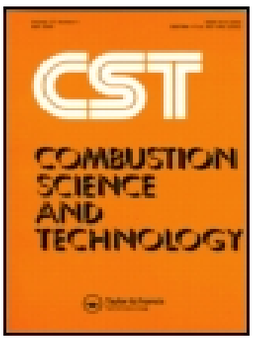

Combustion Science and Technology

ISSN: 0010-2202 (Print) 1563-521X (Online) Journal homepage: https://www.tandfonline.com/loi/gcst20

Numerical Study on the Combustion Process of n-heptane Spray Flame in Methane Environment Using Large Eddy Simulation

Wanhui Zhao, Lei Zhou, Zongkuan Liu, Jiayue Qi, Zhen Lu, Haiqiao Wei & Gequn Shu

To cite this article: Wanhui Zhao, Lei Zhou, Zongkuan Liu, Jiayue Qi, Zhen Lu, Haiqiao Wei & Gequn Shu (2019): Numerical Study on the Combustion Process of n-heptane Spray Flame in Methane Environment Using Large Eddy Simulation, Combustion Science and Technology, DOI: 10.1080/00102202.2019.1655404

To link to this article: https://doi.org/10.1080/00102202.2019.1655404

Published online: 21 Aug 2019.

COMBUSTION SCIENCE AND TECHNOLOGY
https://doi.org/10.1080/00102202.2019.1655404

Taylor & Francis
Taylor & Francis Group

Numerical Study on the Combustion Process of n-heptane Spray Flame in Methane Environment Using Large Eddy Simulation

Wanhui Zhao[a], Lei Zhou[a], Zongkuan Liu[a], Jiayue Qi[a], Zhen Lu[b], Haiqiao Wei[a], and Gequn Shu[a]

[a]State Key Laboratory of Engines, Tianjin University, Tianjin, China; [b]Clean Combustion Research Center, King Abdullah University of Science and Technology (KAUST), Thuwal, Saudi Arabia

ABSTRACT

Large eddy simulation is applied for the combustion process of n-heptane spray flame in methane environment. The influence of methane (CH_4) concentration on the auto-ignition process and flame structures are discussed in detail. By increasing the CH_4 concentration in the ambient gas, auto-ignition is delayed obviously at a low initial temperature because of the delayed first-stage ignition. While at a high temperature, the auto-ignition time is less influenced by the addition of CH_4. However, after the addition of CH_4, the concentration of the mixture where the high-temperature ignition is initialed becomes much richer and it is independent of the initial temperatures. In addition, the chemical explosive mode analysis (CEMA) method shows that the mixture in high-temperature regions is non-explosive without CH_4 addition, and the abrupt transition between the explosive and non-explosive mixture at the tip of the reacting spray is observed by adding CH_4 in the ambient gas, indicating that a flame front is developing downstream. This flame front exists for a long time at low CH_4 concentration. The eigenvalue of the Jacobian matrix for the CH_4/air mixture in the ambient gas is increased significantly with the addition of CH_4, indicating that the combustion process is dominated by auto-ignition. Finally, results show that the development of the flame is accelerated by the addition of CH_4 in the ambient gas.

ARTICLE HISTORY
Received 4 November 2018
Accepted 9 August 2019

KEYWORDS
Chemical explosive mode analysis; dual-fuel combustion; ignition; low-temperature combustion

Introduction

With the growing number of vehicles, the shortage of fossil energy and increasing environmental pollution, there is worldwide interest in the use of natural gas engines for their rich resources, widespread distribution infrastructure, low cost, and clean-burning qualities (Li et al. 2017). Furthermore, natural gas is not prone to knock due to its high octane number (Fu et al. 2017), and thus it can achieve high efficiency with relatively high compression ratio. However, it suffers from poor ignition characteristics when natural gas in diesel engine is used due to the low cetane number and high auto-ignition temperature compared with diesel fuel. Previous studies found that the addition of small amounts of n-heptane can shorten the

CONTACT Lei Zhou lei.zhou@tju.edu.cn State Key Laboratory of Engines, Tianjin University, 92 Weijin Road, Nankai District, Tianjin, P. R. China; Haiqiao Wei whq@tju.edu.cn State Key Laboratory of Engines, Tianjin University, 92 Weijin Road, Nankai District, Tianjin, P. R. China
Color versions of one or more of the figures in the article can be found online at www.tandfonline.com/gcst.

ignition delay time of methane-air mixtures (Schlatter et al. 2012, 2016). Therefore, the dual fuel engine, in which pilot diesel ignition is used to trigger high-temperature ignition, is applied to ensure reliable combustion initiation.

However, dual fuel engine exists knock at high loads and the incomplete gaseous fuel utilization at relatively light loads. To ensure the stable combustion and realize low emission, a better understanding of the combustion process of dual fuel engine is necessary. Many experimental and numerical studies have been done in different combustion devices (Daca and Gülder 2017; Schlatter et al. 2016; Wu, Rutland, Han 2019; Yousefi, Birouk, Guo 2017b; Zhang et al. 2018), finding that the presence of methane in the ambient gas has delayed the auto-ignition of n-heptane (Schlatter et al. 2016) and both the pre-ignition and post-ignition processes are influenced in a complex manner depending on CH_4 concentration and the operating conditions (Papagiannakis and Hountalas 2004). In addition, the influences of methane content in the ambient gas, the initial temperatures, pilot fuel mass (Schlatter et al. 2016), and diesel injection timing (Yousefi, Birouk, Guo 2017a) on the dual-fuel combustion have been studied. Recently, Srna et al. (2019) conducted experiments to investigate the low- and high-temperature ignition stages based on laser diagnostics for formaldehyde detection in a rapid compression-expansion machine (RCEM). N-dodecane was directly injected into the chamber with premixed methane and the mixture was compressed by the piston with a high speed. Results show that the first formaldehyde (CH_2O) detection for the two cases with similar ignition delay time is found almost constant regardless of methane content. However, the types of data obtained from the experiments are still limited by the measurement techniques. For simulation studies, the effects of pressure, temperature, the equivalence ratio of the homogenous mixture, and mixing layer thickness of the n-heptane/methane–air mixture on the flame development process have been investigated previously (Wang and Abraham 2015). Three components to the characteristic time required for steady premixed flame were considered, including the time for auto-ignition to occur, time for peak temperature to be achieved following auto-ignition, and time for steady flame propagation in the premixed fuel/air mixture to be achieved. Demosthenous et al. (2016) investigated the auto-ignition of n-heptane sprays in methane/air mixture and the subsequent ignition of methane premixed flame in a constant volume configuration using direct numerical simulation. Results show that the amount of n-heptane has great influence on the methane oxidation behavior which follows roughly an auto-ignition regime and a canonical premixed flame for large and small amounts of n-heptane respectively. Moreover, Li et al. (2017) numerically investigated the combustion process of the natural gas-diesel dual-fuel engine. For such investigation, diesel was directly injected into the cylinder, while methane was injected into the intake port. The results show that the momentum produced by the direct injection and combustion pushes the combustion products toward the unburned methane-air mixture region, as a result of which, the mixing between the hot combustion products and cold unburned methane/air is improved. Previous studies are limited to investigate the effect of diesel fuel spray on the combustion of methane, and the dominant factor in controlling the combustion processes for dual-fuel is not well understood.

Therefore, the objective of this work is to investigate the combustion characteristics of n-heptane spray flame in the presence of methane-air mixture under various ambient conditions. The new contributions of this work are summarized as below. Firstly, to

comprehensively study how the combustion process of turbulent n-heptane spray flames is affected by different methane concentrations in the ambient gas using large eddy simulation. Secondly, to study the effect of initial gas temperature and methane concentration on the low-temperature combustion process and the distributions of key species, namely CH_2O, hydroxide (OH), and acetylene (C_2H_2). Thirdly, to investigate the dominant role in controlling the combustion process of dual-fuel, and the differences between the auto-ignition of n-heptane and dual-fuel combustion using the chemical explosive mode analysis (CEMA) method. Finally, the effect of the initial temperature, oxygen concentration and methane addition with and without changing the oxygen concentration on the ignition process is carefully analyzed.

The present study is organized as follows: The numerical setup is shown in Section 2. Discussion of the combustion processes at different CH_4 concentrations in the ambient gas and the combustion modes, including auto-ignition and flame development, are shown in Section 3, and finally, Section 4 summarizes the present work and gives the main conclusions.

Numerical setup

Methodology

The numerical scheme of the employed program is based on the Arbitrary Lagrangian-Eulerian method with the finite volume method (Amsden 1997). For the continuum phase in LES, a third-order Monotone Upstream-centered Schemes for Conservation Laws (MUSCL) (van Leer 1974) is implemented to obtain high order accuracy for the convection term. In our previous studies (Wei et al. 2018c; Zhou et al. 2015), the effects of the numerical differencing scheme on the non-reacting spray structures and ignition process of turbulent spray flames are discussed in detail. To describe the effects of the filtered small-scale turbulence, a k-equation sub-grid turbulent kinetic energy model with $C_\mu = 0.067$ and $C_\varepsilon = 0.916$ (Sone and Menon 2003) has been implemented. The present KIVALES version is further extended to include the subgrid scalar mixing model linear eddy simulation (denoted hereafter, as LES-LEM (Sone and Menon 2003) method). The LEM model offers a fundamentally different closure for the scalar fields within the context of LES. In LEM, subgrid turbulent mixing and molecular diffusion processes evolve concurrently in a one-dimensional domain within each LES cell.

In the LES-LEM approach, the velocity is constituted from three parts: a filtered LES-resolved part $\tilde{u}_j$, an LES-resolved sub-grid fluctuation (calculated from the sub-grid turbulent kinetic energy k^{sgs}) $u_j^{'}$ and an unresolved sub-grid fluctuation $u_j^{''}$ (Sone, Patel, Menon 2001). The instantaneous velocity can be written as $u_j = \tilde{u}_j + u_j^{'} + u_j^{''}$. The spatial filter length Δ is derived from the size of the cell. The governing equations including mass, energy, species conservation, and the Navier-Stokes equations are listed below.

$$\frac{\frac{\partial \bar{\rho}}{\partial t} + \partial \tilde{\rho} \tilde{u}_j}{\partial x_j = \overline{\dot{\rho}^s}} \tag{1}$$

$$\frac{\partial \bar{\rho}\tilde{u}_j}{\partial t}+\frac{\partial(\bar{\rho}\tilde{u}_i\tilde{u}_j)}{\partial x_j}=-\frac{\partial \bar{p}}{\partial x_i}+\frac{\partial \bar{\tau}_{ij}}{\partial x_j}-\frac{\partial \tau_{ij}^{sgs}}{\partial x_j}+\overline{F_i^s} \tag{2}$$

$$\frac{\partial \bar{\rho}\tilde{e}}{\partial t}+\frac{\partial \bar{\rho}\tilde{u}_j\tilde{e}}{\partial x_j}=-\bar{p}\frac{\partial \tilde{u}_j}{\partial x_j}-\frac{\partial h_j^{sgs}}{\partial x_j}-\frac{\partial \overline{q_j}}{\partial x_j}+\overline{\tau_{ij}}\frac{\partial \tilde{u}_i}{\partial x_j}+\Theta^{sgs}+\overline{\dot{Q}^c}+\overline{\dot{Q}^s} \tag{3}$$

$$\frac{\partial \rho Y_m}{\partial t}+\frac{\partial}{\partial x_j}\left[\rho\left(\tilde{u}_j+u_j^{'}+u_j^{''}\right)Y_m\right]=\frac{\partial}{\partial x_j}\left(\rho D_m\frac{\partial Y_m}{\partial x_j}\right)+\dot{\rho}_m^c+\dot{\rho}_m^s \tag{4}$$

In the equations above, the variables ρ, u, and t are the density, velocity, and time respectively, while e, Y_m, p, and D_m represent the internal energy, mass fraction of species m, pressure, and diffusion coefficient, respectively. The variables $\tau_{i,j}$, q_j, h_j^{sgs}, and Θ^{sgs} refer to the stress tensor, heat flux sub-grid scale enthalpy flux, and sub-grid viscous work respectively. In Equations (2) and (3), the superscript *sgs* stands for the sub-grid scale variables. $\overline{F_i^s}$ is the filtered drag force acting on the gas phase from the liquid. $\overline{\dot{Q}^c}$ and $\overline{\dot{Q}^s}$ in Equation (3) show the contributions of chemical reaction and spray to the internal energy respectively. $\dot{\rho}^c$and $\dot{\rho}^s$ in Equation (4) represent the source terms owing to chemical reactions and spray, respectively.

The filtered stress tensor $\bar{\tau}_{ij}$ and the sub-grid scale stress $\bar{\tau}_{ij}^{sgs}$ are calculated by

$$\bar{\tau}_{ij}=-\bar{p}\delta_{ij}+2\overline{\rho\nu}\left(\bar{S}_{ij}-\frac{1}{3}\bar{S}_{kk}\delta_{ij}\right) \tag{5}$$

$$\bar{\tau}_{i,j}^{sgs}=-2\bar{p}\nu_t\left(\bar{S}_{ij}-\frac{1}{3}\bar{S}_{kk}\delta_{ij}\right)+\frac{2}{3}\bar{\rho}k^{sgs}\delta_{ij} \tag{6}$$

where $\bar{S}_{ij}$ and ν_t are the filtered strain rate tensor and the eddy viscosity, respectively. They are defined as

$$\bar{S}_{ij}=\frac{1}{2}\left(\frac{\partial \tilde{u}_j}{\partial x_i}+\frac{\partial \tilde{u}_i}{\partial x_j}\right) \tag{7}$$

$$\nu_t=C_\nu k^{sgs1/2}\bar{\Delta}\ ,\ \text{with}\ C_\nu=0.067 \tag{8}$$

The sub-grid turbulent kinetic energy k^{sgs} is calculated from the turbulent kinetic energy equation

$$\frac{\partial \bar{\rho}k^{sgs}}{\partial t}+\frac{\partial \bar{\rho}\,\tilde{u}_j\,k^{sgs}}{\partial x_j}=-\tau_{ij}^{sgs}\frac{\partial\,\tilde{u}_j}{\partial x_j}-D^{sgs}+\frac{\partial}{\partial x_j}\left(\bar{\rho}\frac{\nu_t}{\mathrm{Pr}_t}\frac{\partial k^{sgs}}{\partial x_j}\right) \tag{9}$$

In the above equation, the sub-grid energy dissipation rate is computed by

$$D^{sgs}=C_\varepsilon\bar{\rho}(k^{sgs})^{3/2}/\bar{\Delta},\ \text{with}\ C_\varepsilon=0.916 \tag{10}$$

The Prandtl number Pr_t is set as 0.74 here. $\bar{q}_j$ stands for the filtered heat conduction and it is defined as:

$$\bar{q}_j = -\bar{K}\frac{\partial \tilde{T}}{\partial x_j} - \bar{\rho}\sum_{m=1}^{N}\tilde{h}_m\tilde{D}_m\frac{\partial \tilde{Y}_m}{\partial x_j} \tag{11}$$

In the LES-LEM method, the molecular diffusion and sub-grid turbulent stirring are solved in the sub-grid LEM cells within each LES cell. The convection term on large scale is computed in the resolved field based on the turbulent fluctuation velocity u', with $u' = \sqrt{\frac{2}{3}k^{sgs}}$. Equation (4) is resolved by two sub-steps, and it can be rewritten as

$$\frac{Y_m^* - Y_m^n}{\Delta t} = -u_j^{''}\frac{\partial Y_m}{\partial x_j} + \frac{1}{\rho}\frac{\partial}{\partial x_j}\left(\rho D_m\frac{\partial Y_m}{\partial x_j}\right) + \dot{\rho}^c + \dot{\rho}^s \tag{12}$$

$$\frac{Y_m^{n+1} - Y_m^*}{\Delta t} = -\left(\tilde{u}_j + u_j^{'}\right)\frac{\partial Y_m}{\partial x_j} \tag{13}$$

where Y_m^* is the mass fraction of species m in the intermediate stage. Then Equation (12) is solved in a one-dimensional LEM domain and stands for the sub-grid processes, which can be rewritten as

$$\frac{\partial Y_m}{\Delta t} = \frac{1}{\rho}\frac{\partial}{\partial s}\left(\rho D_m\frac{\partial Y_m}{\partial s}\right) + F_m^{stir} \tag{14}$$

In the equation above, s stands for the coordinate in the LEM domain. The time step Δt_{diff} to integrate this equation is determined by

$$\Delta t_{diff} = C_{diff}\frac{(\Delta s)^2}{\max(\nu, D_m)} \tag{15}$$

where C_{diff} is set as 0.25 and Δs represents the size of the LEM grid.

The effect of turbulent stirring in the sub-grid, F_m^{stir}, is implemented by a stochastic rearrangement of the scalar field in the LEM domain, known as *triplet maps* (Kerstein 1989). This process shows the stirring effect of eddies that are smaller than the LES cells. These events evolve two characteristic parameters: the mapping frequency and the probability function of the eddy size l in the sub-grid and they are defined as

$$f(l) = \frac{5}{3}\frac{l^{-\frac{8}{3}}}{\eta^{-\frac{5}{3}} - \bar{\Delta}^{-\frac{5}{3}}} \tag{16}$$

$$\Lambda = \frac{54}{5}\frac{\nu \mathrm{Re}^{sgs}}{\bar{\Delta}^3}\frac{(\bar{\Delta}/\eta)^{5/3} - 1}{1 - (\eta/\bar{\Delta})^{4/3}} \tag{17}$$

where η is the Kolmogorov length scale. The sub-grid Reynolds number is determined by $\mathrm{Re}^{sgs} = u'\bar{\Delta}/\nu$. The stirring time step is defined by

$$\Delta t_{stir} = \frac{1}{\Lambda\bar{\Delta}} \tag{18}$$

Numerical conditions

The discrete droplet model (DDM) (Amsden 1997) is applied for the discrete phase. The droplet particles were tracked by solving the droplet velocity, mass, and temperature equations using the Lagrangian method. The Kelvin-Helmholtz Rayleigh-Taylor (KH-RT) model (Patterson and Reitz 1998) is used to predict the primary and secondary liquid breakups processes. In the KH-RT model, the two model parameters B_0 and B_1 are set to be 0.61 and 18.0, respectively. And O'Rourke (1981) model is employed for the simulation of the collision and coalescence. The interactions between the two phases are described through a two-way coupling, i.e. "gas-to-liquid" and "liquid-to-gas". In "gas-to-liquid", the changes of the droplet velocity in the computation domain are attributed to the drag force $F_{i,d}$ on the droplet and calculated by the relative velocity between the droplet and the gas. In the "liquid-to-gas" aspect, the effects of liquid motion on the gas phase are treated as the Lagrangian source terms in the Eulerian momentum equation. Note that in LES the subgrid dispersion velocity model (Zhou et al. 2011) is employed to calculate the effects of turbulent flows on droplets. Furthermore, the spray source term model (Bharadwaj, Rutland, Chang 2009) with a twice-test filtering subgrid gas velocity treatment is used to deal with spray effects on the subgrid turbulent kinetic energy.

This work is focused on the investigation of the ignition characteristics and flame structures of the n-heptane spray with methane in the ambient gas. In order to simulate the combustion process, parallel computation of detailed chemistry using the Message-Passing Interface (MPI) has been implemented into KIVALES (Wei et al. 2018c). MPI allows for chemistry to be computed in parallel on multiple CPUs. This process is accomplished at each computational time step. Once combustion occurs and chemical kinetic calculations start, KIVALES transfers information on the temperature, pressure, and compositions of each cell to CHEMKIN, where chemical reactions are computed on a number of CPUs using decomposed uniform grids. Therefore, in the present study, the chemical reactions are solved on LES cells based on the average composition, pressure, and temperature. This method has also been applied for the simulation of non-premixed hydrogen jet flames by Martinez et al. (2014). The computational domain is a cylinder with 30 mm in diameter and 100 mm in height, as shown in Figure 1. A no-slip boundary condition is applied to all boundaries of the walls in this work. The time step ranges from 1.0×10^{-8} to 1.0×10^{-6} s. N-heptane is injected into the cylinder at the top center along the axial direction. The total mesh is nearly 0.8 million. The injection pressure is 150 MPa. Fuel temperature is 373 K. The ambient gas density is 14.8 kg/m^3. The ambient gas pressure is changed based on the experiments from Pickett (2019), Pickett and Siebers 2004). The simulated conditions and the parameters of diesel spray are shown in Tables 1 and 2, respectively. The basic cases, i.e. B1, B2, and B3 without methane addition are consistent with the experiments on the Engine Combustion Network (ECN) website (Pickett 2019). Six different cases with different CH_4 concentrations in the ambient gas are compared.

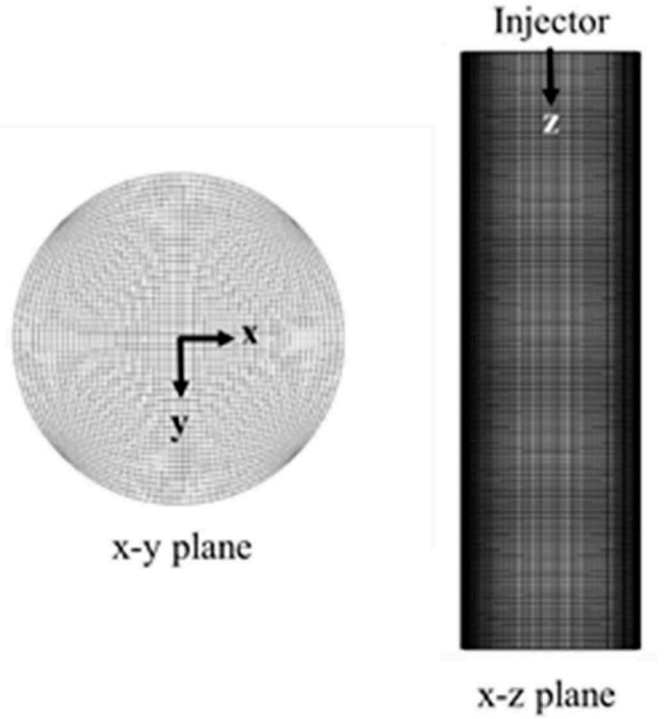

Figure 1. Schematic of the computational mesh in the top (left) and side (right) views.

Table 1. Simulation settings.

Case	ϕ_{CH4}	T (K)	P(MPa)
B1	0	850	3.58
B2		1000	4.21
B3		1200	5.06
1	0.5	850	3.58
2		1000	4.21
3		1200	5.06
4	1.0	850	3.58
5		1000	4.21
6		1200	5.06

Table 2. Parameters of diesel spray.

Fuel	n-heptane
Hole diameter(mm)	0.1
Injection duration (ms)	6.8
Injection pressure (MPa)	150
Fuel mass (mg)	17.8
Gas density (kg/m^3)	14.8
Temperature of fuel (K)	373

For example, $\phi_{CH4} = 0.5$ means that the equivalence ratio of CH_4 and oxygen in the initial ambient gas is 0.5.

In this work, the reduced mechanism of Liu et al. (2004) including 44 chemical components was used for simulating the ignition process of liquid fuel n-heptane in the

presence of methane. This mechanism was validated in terms of the ignition delay times for the homogeneous mixtures with different equivalence ratios, initial temperatures, and pressures, and it has been successfully used in spray combustion (Irannejad, Banaeizadeh, Jaberi 2015; Wei et al. 2018b) as well as the simulation for methane/n-heptane dual-fuel combustion (Demosthenous et al. 2016). The performance of the present mechanism in predicting the auto-ignition process of methane was compared with the detailed methane mechanism (GRI 3.0 (Smith)) in Ref (Wei et al. 2018a). The results calculated from the 44-species mechanism are in good agreement with the detailed mechanism. The previous study (Irannejad, Banaeizadeh, Jaberi 2015) also showed that the low-temperature chemistry was included in the present mechanism even at an initial temperature of 800 K. Moreover, Soriano et al. (2017) also verified the present kinetic mechanism in capturing the flame speed of methane/n-heptane dual fuel. The predicted results are in good agreement with experimental data over a wide range of methane concentrations. Therefore, this mechanism developed by Liu et al. can be used for n-heptane spray auto-ignition problems containing methane.

Results and discussion

Model validation

Non-reacting spray

In this work, we applied the LES-LEM method to investigate the ignition process and flame structures of methane/n-heptane dual fuel at different CH_4 concentrations in the background. Parameters of spray models remained constant regardless of CH_4 concentrations. The spray models were validated by comparing the predicted liquid and vapor penetrations of n-heptane spray with the experimental data under the non-reacting condition. The experimental data can be found on the ECN website (Pickett 2019). In our previous study (Wei et al. 2018b), we have compared the mixture fraction distributions at different locations and times from the present mesh with those from a finer mesh. The total cell number of the fine mesh is 1.6 million. Results showed that the present mesh can give a reasonable estimation. Moreover, we have also evaluated the quality of the present mesh under the non-reacting condition by comparing the results from approximately 30 realizations (Wei et al. 2018c). The ratio between the resolved and total turbulent kinetic energy (TKE) revealed that high-levels of TKE can be resolved by the present mesh, especially at downstream positions. Here, we give a comparison of the predicted penetration lengths with the experimental data, as shown in Figure 2. The liquid penetration length is defined as the maximum distance from the axial position with 95% injected fuel mass to the injection location, and the vapor penetration length is defined as the distance from the farthest location with 0.1% fuel mass fraction to the nozzle exit. It can be seen from Figure 2 that the simulation is capable of reproducing the spray penetration, although the vapor penetration is a bit over-prediction before 1.0 ms after the start of injection (ASOI). The contour of the mass fraction is compared with the instantaneous experimental image obtained using Rayleigh scattering imaging (Idicheria and Pickett 2007). Qualitative comparison between the measured and predicted results can be seen. Hence, the present numerical model can be used to study the spray structures and ignition process of n-heptane spray even after CH_4 is contained in the initial gas.

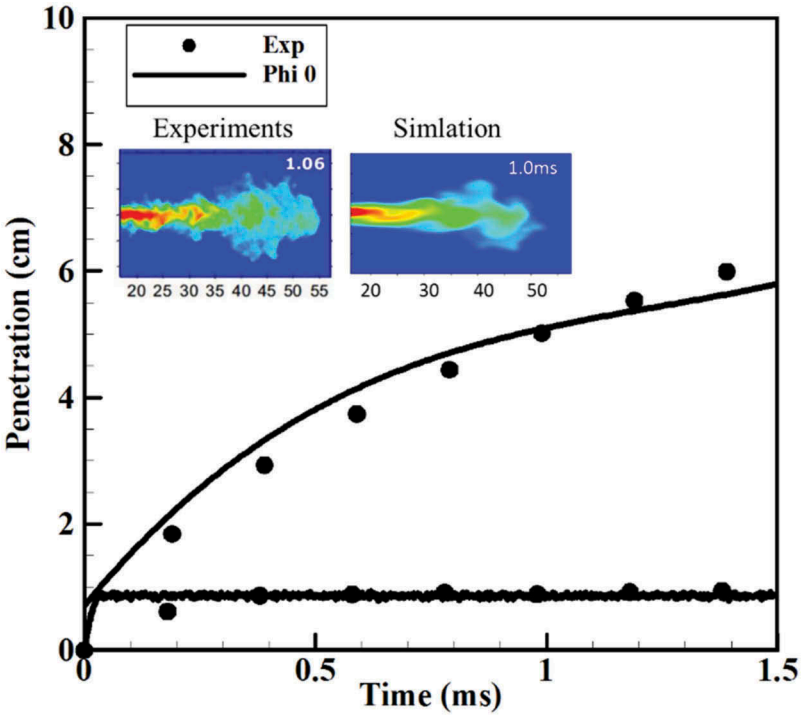

Figure 2. Comparisons of liquid and vapor penetration lengths.

Reacting spray

Ignition delay (ID) is a key parameter for the diesel spray flames because ID directly influences the combustion phasing. The ID invested in this study is defined as the time when the maximum temperature in the domain reaches the ignition temperature T_{ig}, which is calculated by $T_{ig} = 0.5 \times (T_{amb} + T_{max})$ (Bekdemir et al. 2013). T_{amb} and T_{max}represent the initial ambient temperature and the maximum temperature in the computational domain, respectively. And the location of the flame lift-off length (LOL) is defined as the most upstream position with the temperature equal to T_{ig}. Figure 3 shows that the predicted flame structures including mixture fraction (Z), temperature (T), and OH contours are compared with the chemiluminescence image from (Pickett 2019) at an initial temperature of 850 K, which represents the typical gas temperature in low-temperature combustion strategies. The results show that the predicted flame LOL agrees well with the measured one, while the flame head is slightly underestimated. It may attribute to the overestimation of the ignition delay time (shown in Figure 4), because the earlier appearance of the low- and high-temperature reactions contributes to the acceleration of the flame head (Zhou, Zhao, Wei 2018), as demonstrated by the experiments (Desantes et al. 2014).

Ignition delay times at different CH_4 concentration

The predicted and measured IDs for the reacting spray at different CH_4 concentrations are shown in Figure 4. For the cases without CH_4 in the ambient gas, the simulated IDs are

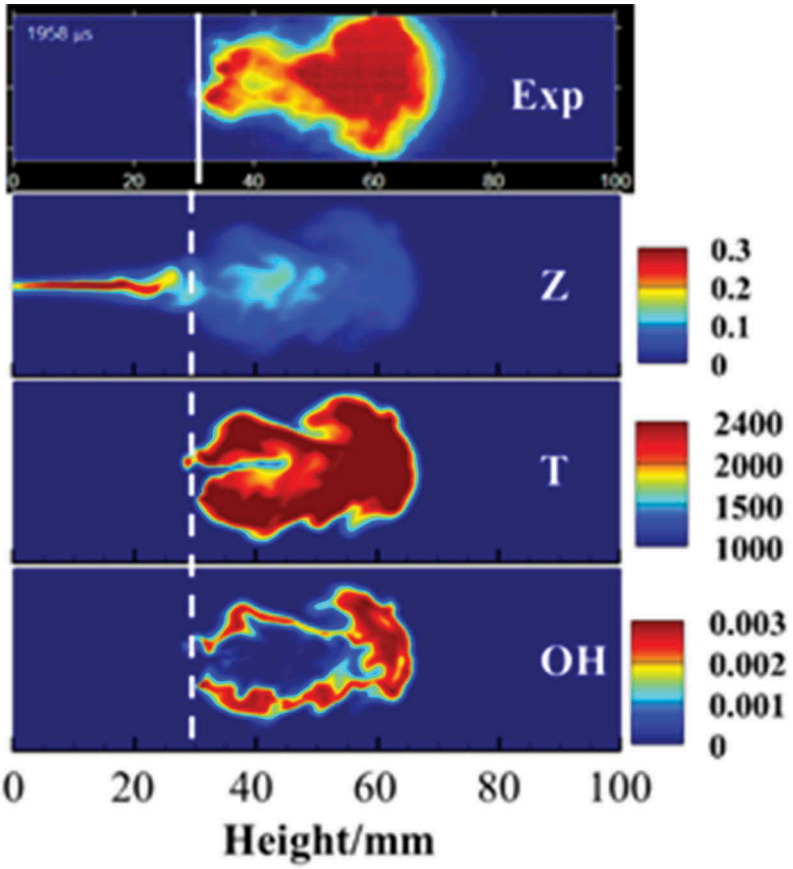

Figure 3. Comparisons of the predicted and measured flame structures in terms of mixture fraction (Z), temperature (T) and OH mass fraction at 850 K without methane addition. Experiments from (Pickett 2019). The white solid and dashed lines represent the locations of the flame LOL.

overestimated at low temperatures compared to the experiments from the ECN website (Pickett 2019). The predicted results agree well with experimental data at high temperatures. When CH_4 is added to the initial ambient gas, ID increases rapidly, especially at low temperature. While at high temperatures, the effect of methane addition on the IDs is negligible because methane addition prolongs the first-stage ignition, but only marginally at high temperatures, at which the mixture reactivity is still very high (Srna et al. 2019). Therefore, the influence of the addition of CH_4 on the ID is minor. However, at lower temperatures, the first-stage of ignition and low-temperature reactions are more obvious. Although the different methane content is different, the first CH_2O detection and high-temperature ignition can be distinguished. The addition of CH_4 significantly prolongs the first-stage ignition process. Srna et al. (2019) found that particularly in the fuel-lean mixture, the inhibition effect on the low- and high-temperature reactions is much more obvious.

An increasing trend in ID can be found when methane is included in the initial ambient gas, as shown in Figure 4. Previous studies (Aggarwal, Awomolo, Akber 2011; Karim 2003) have shown that the prolonging effect of the ignition delay by the addition of

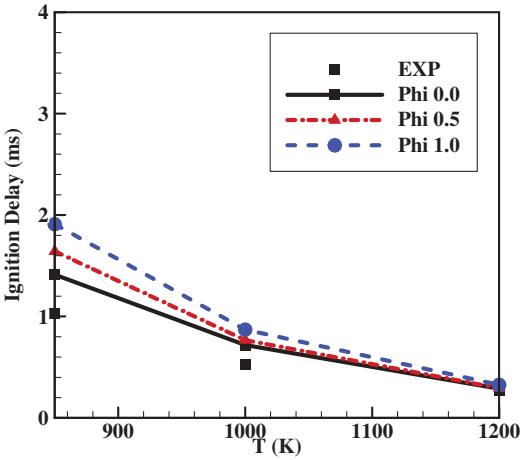

Figure 4. Comparisons of ignition delay times at different initial temperatures and methane concentrations.

methane can be attributed to two reasons: one is the reduction of oxygen, and the other is the effect of the high specific heat capacity and reactions of CH_4 owing to CH_4 addition. To analyze the mechanism, three groups including six cases are conducted by CHEMKIN-PRO 15131 (2013) using a homogeneous reactor as shown in Figure 5. In each group, equivalence ratios of n-heptane to oxygen are set to $\phi_{c7} = 1.0$ and $\phi_{c7} = 2.0$. For the first group, no CH_4 is included in the air. For the second group, n-heptane is oxidized in the methane/air environment, where the volume of air is replaced by CH_4 with the same volume and the mole ratio between CH_4 and O_2 in the ambient gas is 1/2. Therefore, the proportion of oxygen, nitrogen and methane is 19%, 71.5%, 9.5% respectively. For the third group, the volume of CH_4 in the second two cases is replaced by N_2 to investigate the effect of CH_4 addition. The effect of N_2 is ignored, because it is negligible in this work. Hence, the effect of oxygen reduction can be seen via comparing the first and third cases,

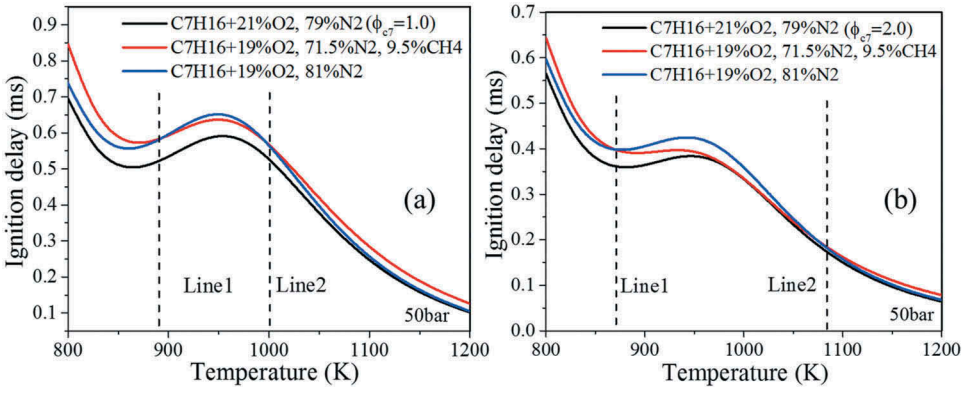

Figure 5. Effects of CH_4 addition and oxygen reduction on the ID. The equivalent ratios of n-heptane to oxygen in the cases without CH_4: (a)$\phi_{c7} = 1.0$; (b)$\phi_{c7} = 2.0$. Here, ϕ_{c7} is calculated based on the oxygen content in the initial gas.

and the effect of CH_4 addition can be seen by comparing the second and third cases. There are two vertical dashed lines in Figure 5, which show the critical points of the contributions of CH_4 addition or oxygen reduction on the ignition delay. In low-temperature regions, on the left side of Line 1, the addition of CH_4 plays a more important role in prolonging the ID. On the right side of Line 2, the effects of both CH_4 addition and oxygen reduction are negligible. In the intermediate temperature regions, the ID is delayed more obviously owing to the lack of oxygen. It should be noted that the fuel temperature is basically greater than 900 K after injection, and thus, it can be concluded that the longer ignition delay is mainly caused by the reduction in the oxidizer concentration. Moreover, the ID in the system is determined by the successful collisions, which means that if it reaches the activation energy of the reaction, the collision is successful. As the bonds of methane is much stronger than that of n-heptane, the decomposition of methane is much slower. With the presence of methane, the molecule collisions are limited by the high activation energy of these reactions (Levine 2009). At a high initial temperature of 1200 K, it is much easier to reach the activation energy and trigger the high-temperature reactions. By adding more methane in the ambient gas, the slow decomposition increases the ID for n-heptane (Ghaderi Masouleh et al. 2017).

Overall combustion process at different CH_4 concentrations

Fuel evaporation

The effect of methane concentration on the consumption of n-heptane at different initial temperatures is shown in Figure 6. It can be seen that the main difference appears at the time approaching the ID. Once the auto-ignition of n-heptane occurs, n-heptane is rapidly consumed. By decreasing the initial temperature, the difference becomes more obvious. This is because the ignition delay time is significantly prolonged with the presence of methane in the ambient gas at an initial temperature of 850 K. Meanwhile, the fuel consumption by low- and high-temperature reactions also becomes significantly slow, resulting in that more n-heptane is accumulated in the computational domain, especially for the case with a methane concentration of unity. Also, it is confirmed by the experiments that the premixed methane inhibits the reactivity of the mixture, and thus the high-temperature ignition triggered by n-heptane is prolonged (Schlatter et al. 2016). Recently, Demosthenous et al. (2016) conducted a direct numerical simulation of spray auto-ignition in methane-air mixtures finding that the evaporation and mixing of the cold n-heptane fuel with ambient gas are the dominant processes prior to ignition. Then the fuel molecule breaks up into R radical through the H-atom abstraction at a low temperature or decomposes into small molecule at a high temperature (Zhang et al. 2016). Moreover, the oxidization and ignition processes of n-heptane/methane dual fuel are also dependent on the injected n-heptane quantity (Demosthenous et al. 2016). If enough n-heptane is injected into the chamber, the ignition of the dual fuel is dominated by the n-heptane auto-ignition kernels. It is worth noting that at 1200 K, IDs are slightly affected by the methane concentration. The high-temperature reactions occur much earlier than that at low initial temperatures, and consequently, the accumulation of n-heptane mass is quickly reduced. It is also interesting that after the auto-ignition of n-heptane at an

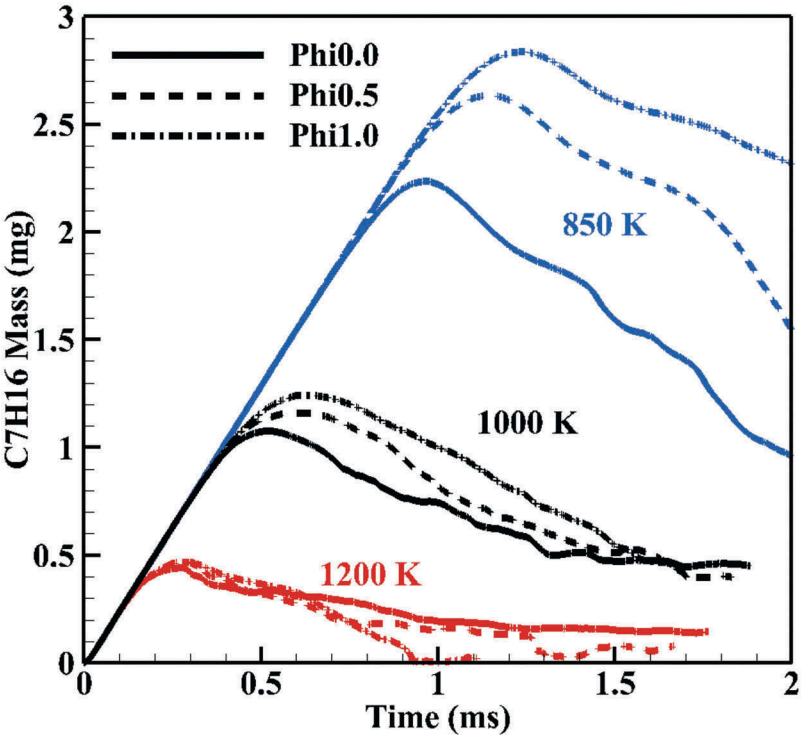

Figure 6. Temporal evolutions of n-heptane mass at different initial temperatures. (Different colors represent different initial temperatures).

initial temperature of 1200 K, the fuel consumption gradually accelerates in the cases with the presence of methane. This phenomenon is caused by the high-temperature reaction of methane, which expands the high-temperature regions, thereby providing enough energy to enhance the evaporation and decomposition of n-heptane spray.

Combustion at low and high temperatures

In this section, the ignition and combustion processes of dual fuel are further compared at low and high initial gas temperatures. The effect of methane content is also considered. The temporal evolutions of temperature in mixture fraction (Z) space at different CH_4 concentrations are shown in Figure 7, which is derived from the edge of the mixture fraction versus temperature maps and represents the maximum temperature for the mixture with the same equivalence ratio. The profiles are shown at different times after ID, known as $t^* = t - t_{ig}$, where t_{ig} equals to the ID. Z is calculated based on the elemental carbon and hydrogen mass fraction (Irannejad, Banaeizadeh, Jaberi 2015), and is calculated by:

$$Z = \sum_{\alpha=1}^{Ns} \left(MW_C n_{C,\alpha} + MW_H n_{H,\alpha}\right) \frac{Y_\alpha}{MW_\alpha} \tag{19}$$

where MW_C, MW_H, and MW_α are the molecular weights of carbon atoms, hydrogen atoms, and species α respectively. $n_{C,\alpha}$ and $n_{H,\alpha}$ are the number of C and H atoms. Y_α is the mass fraction of species α. Significant differences in the ignition process can be seen in

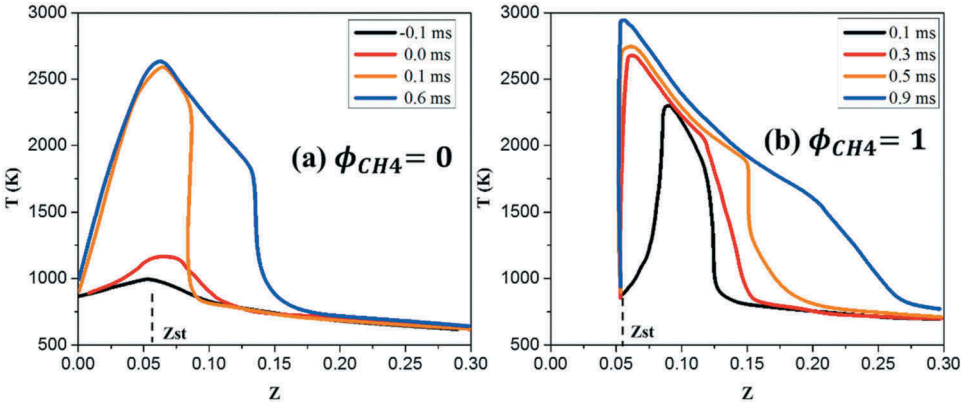

Figure 7. Temporal evolutions of temperature in Z space at different CH_4 concentrations at an initial temperature of 850 K.

Figure 7. Note that by adding more methane in the ambient gas, the oxygen concentration is slightly reduced. As a result, the value of the stoichiometric mixture fraction (Zst) is slightly reduced (Azimov, Kim, Bae 2010). When there is no CH_4 in the initial ambient gas, the heat is released at both fuel-lean and fuel-rich regions before the ID. Once high-temperature kernels appear, the maximum temperature increases very quickly. At later times, the maximum temperature remains almost constant when the high-temperature zones move upstream toward the fuel-rich regions. At a higher CH_4 concentration, ignition moves from fuel-richer to fuel less rich regions and the combustion temperature reaches the peak value at 0.3 ms after the ID. After that, the maximum temperature increases slightly owing to the oxidation of CH_4. Meanwhile, the temperature of fuel-rich cells increases gradually, indicating that the combustion regions move upstream toward the fuel-rich regions. The basic flame structures in T-Z space can be evaluated at the instant of 0.3 ms after the ID. Reactions in fuel/air mixture are initiated at a low temperature for n-heptane flame due to evaporation. The decrease in the temperature leads to the reduction in the adiabatic flame temperature (not shown here). And the combustion of methane is not influenced by evaporation. The maximum combustion temperature is very close to the adiabatic flame temperature.

Although the combustion process of methane/air mixture ignited by n-heptane micro pilots spray was experimentally performed in an optically accessible Rapid Compression Expansion Machine (Schlatter et al. 2016), the information obtained was very limited. The distributions of scatters in the T-Z space at the time approaching the ID and at 0.3 ms after the ID at different initial temperatures are shown in Figure 8. Each point on the scatter plot corresponds to a value of composition and temperature on each LES cell. It should be noted that the addition of CH_4 increases the values of mixture fraction of the ambient gas, i.e. the minimum value of mixture fraction with different CH_4 concentrations. For non-premixed combustion, the radical and temperature increase preferentially at some mixture fractions, indicating that the mixture firstly ignited could be separated from the stoichiometric. The regions with amounts of n-heptane, i.e. fuel-rich regions, always have a low temperature due to evaporation. Ignition delay is not the shortest. The regions with little n-heptane, i.e. fuel-lean regions, have high enough temperature, but

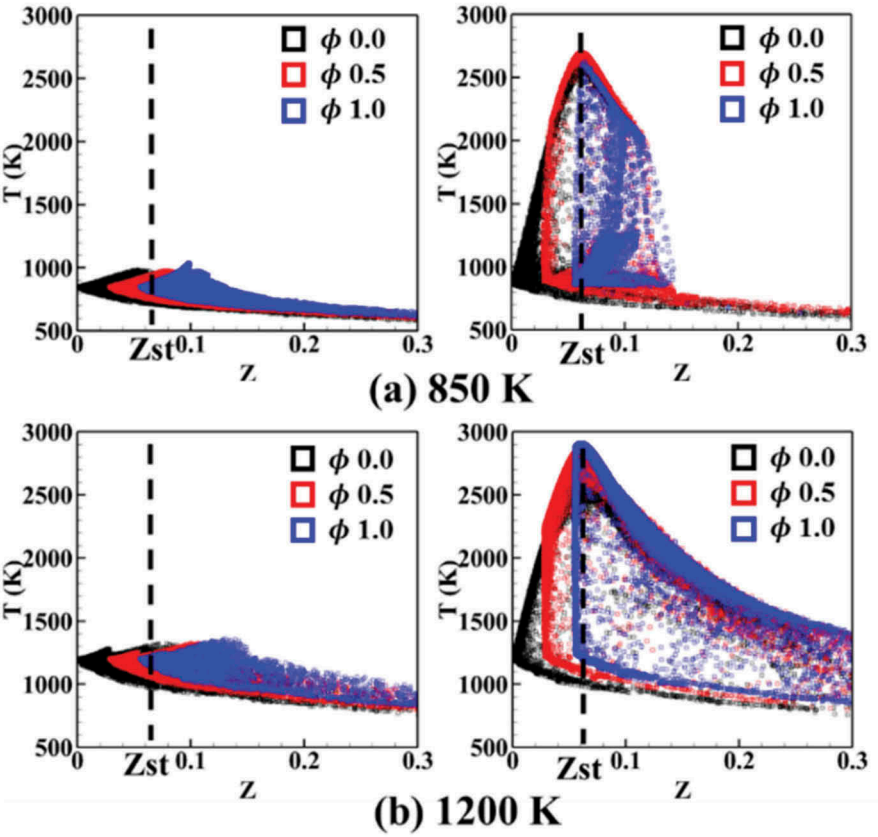

Figure 8. Maps of temperature versus Z with different initial concentrations of CH_4. Left: at t_{ig}. Right: at $t^* = t_{ig} + 0.30$ms. Ambient gas temperatures are (a) 850 K and (b) 1200 K.

they are too lean, and thus the ignition delay is also prolonged. As a result, auto-ignition is initiated at the most reactive mixture fraction regions (Mastorakos 2009), which is always richer than the stoichiometry. Due to the inhibiting effects of the premixed methane on the high-temperature reactions triggered by n-heptane (Schlatter et al. 2016), the mixture reactivity should be high enough to trigger the high-temperature ignition. In addition, it is shown in Figure 5 that as the ignition delay is relatively shorter for fuel-rich regions at the same temperature, the concentration of mixture firstly ignited (Zig) gets richer and Zig is much farther away from stoichiometry at $\phi_{CH4} = 1.0$ than that at $\phi_{CH4} = 0.5$ or 0. By increasing the initial gas temperature, the fuel-richer ignition was observed for n-heptane (Wei et al. 2018b) and n-dodecane (Kundu, Ameen, Som 2017; Pei et al. 2016) spray flames. As shown in Figure 8, the concentration of the mixture firstly ignited gets richer at a higher initial temperature with the same CH_4 concentration. In addition, it is worth noting that the maximum temperature appears in the region of Zst, showing a typical diffusion flame structure regardless of the concentration of CH_4. Since the mixture fraction is calculated based on the elemental carbon and hydrogen mass fraction, the minimum value indicates the concentration of the ambient gas. Due to the presence of CH_4, the minimum mixture fraction doesn't equal to zero. However, the maximum

temperature still appears in the stoichiometric region due to the incomplete combustion at leaner or richer zones. This is of great importance for organizing advanced combustion strategies (Agarwal et al., 2017; Yao, Zheng, Liu 2009) to improve the fuel economy and decrease the pollutant emissions. At 0.30 ms after ignition, i.e. at $t^* = 0.3$ ms, the maximum temperature increases rapidly at high temperatures. By comparing the two figures at $t^* = 0.3$ ms, there are many points locating in the region with mixture fraction ranging from 0.15 to 0.3 at an initial temperature of 1200 K, while only a few points lie in the same region at an initial temperature of 850 K. At a higher initial temperature, the flame plume is smaller and expands less compared to the case at a lower initial temperature. Contacting area between fuel and air is much smaller. Besides, due to the shorter distance between the combustion region and injector, the entrainment of air into the spray is limited. As a result, fuel-richer combustion is observed at a high initial temperature.

To get a further understanding of the combustion processes of n-heptane spray flame in the methane/air mixture, the key intermediate species namely OH, CH_2O and C_2H_2 in the T-Z space are analyzed at 0.30 ms after the ID, as shown in Figure 9. CH_2O marks the ignition process and represents a cool flame, and C_2H_2 can be used as a soot precursor (Pei et al. 2015). Note that only the points with $Y_i > 20\% \times Y_i^{max}$ are shown in Figure 9, where Y_i is the mass fraction of species i, and Y_i^{max} represents the maximum mass fraction of species i in the entire combustion domain. It can be seen that OH, CH_2O and C_2H_2 are mainly distributed in different regions in the T-Z space. For example, at a high CH_4 concentration in the cases with $\phi_{CH4} = 1$, OH is mainly distributed in a narrow zone in the mixture fraction space and in the high-temperature regions. The flame surface is contacting with the ambient gas containing CH_4 and oxidizer. For the cases with more methane addition, as the equivalence ratio in the ambient gas is unity, the oxidizer is quickly consumed by CH_4, and no more oxygen is available near the flame surface. As a result, high levels of C_2H_2 are observed at the locations with a high CH_4 concentration. It can also be seen that with the increase of methane in the ambient gas, the OH distribution transfers to the locations with stoichiometric mixture fraction at 850 K and 1200 K, which is caused by the consumption of methane reaction, such as $CH_4 + OH \rightarrow CH_3 + H_2O$.

The formaldehyde (CH_2O) as an intermediate indicator of the low-temperature combustion has a significant effect on the auto-ignition of CH_4 (Manias et al. 2016). As shown in (Manias et al. 2016), the CH_2O additives associated with the explosive mode can considerably reduce the ignition delay of methane combustion. Therefore, it can be seen from Figure 9a that CH_2O is found in the fuel-lean region without the presence of methane at an initial temperature of 850 K. However, as the methane additives increase in the ambient gas, the CH_2O only appears in relatively low-temperature and fuel-rich regions. This is different from that at a high initial temperature of 1200 K. The high-temperature reactions dominate the combustion of n-heptane spray flame with and without the presence of methane, which reduces the residence time of intermediate species. Only the presence of methane slightly delays the combustion process and at $t^* = 0.30$ ms the CH_2O can be found in low temperature and fuel-rich region, which implies that the present CH_2O is produced by the n-heptane auto-ignition. Overall, the C_2H_2 is mainly produced in fuel-rich regions under different conditions. Especially, for the cases at an initial temperature of 1200 K, C_2H_2 is formed in very rich regions over a wide range of

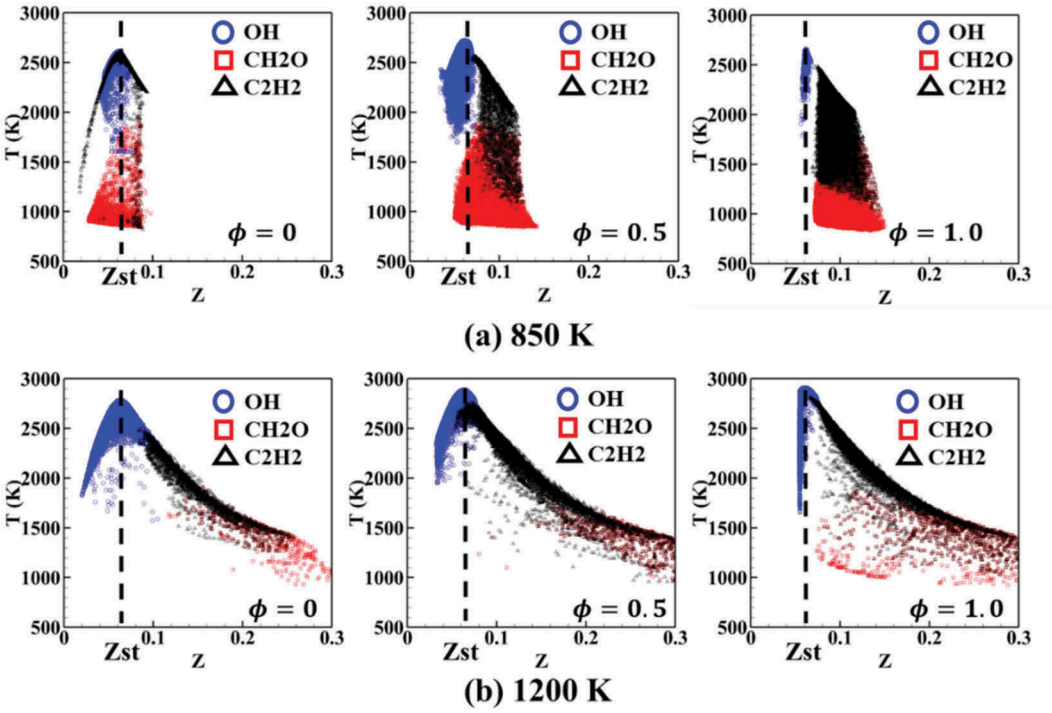

Figure 9. Key species distributions in T-Z space at t* = 0.30 ms.

mixture fraction, owing to the decrease in flame lift-off length (LOL) and the limited mixing time. However, at 850 K, C_2H_2 is clearly formed in both fuel-lean and fuel-rich regions without CH_4 addition at this time. This is because that the mixing between fuel and air is much better and the small value of C_2H_2 is due to the incomplete combustion. Furthermore, the addition of CH_4 leads to the formation of C_2H_2 in low-temperature regions, where the mixture is very rich owing to the lack of oxygen in the air. After the appearance of high-temperature kernels, the momentum produced by the n-heptane injection and combustion pushes the combustion products of fuel injection and methane within the spray flames toward the unburned methane/air mixture. Such a movement enhances the mixing of the hot combustion products and unburned methane/air mixture and dominates the combustion of methane outside of the spray flames (Li et al. 2017). The oxidizer ahead of the flame surface is insufficient for n-heptane combustion with the presence of methane in the ambient gas. Moreover, the entrainment of oxidizer into the spray is also limited due to fuel combustion (García-Oliver et al. 2017). The thinner flame structure at a high initial temperature further limits the interaction between the ambient gas and combustion. As a result, high levels of C_2H_2 are observed at 1200 K.

Chemical explosive mode analysis

The previous section shows the auto-ignition processes at different CH_4 concentrations. In this section, the development of flame structures of n-heptane spray flame with the

presence of methane is further analyzed. Chemical explosive mode analysis (CEMA) is employed to investigate the ignition characteristics of n-heptane spray flames injected into the environment full of methane. Previous studies showed that the ignition, extinction, and flame fronts can be detected by CEMA (Luo et al. 2012; Wei et al. 2019). The CEMA method is briefly summarized here. The Jacobian of the chemical source term, $\mathbf{J}_\omega$, in the governing equations can be used to account for the local chemical characteristics. $\mathbf{J}_\omega$ is defined as $\mathbf{J}_\omega = \partial\omega/\partial y$, where y represents the vector of species concentration and temperature, and ω is the chemical source term. λ_e is the real part of the eigenvalue. A positive value of λ_e indicates that the mixture is explosive while a negative value shows that the mixture has already ignited and is non-explosive. The abrupt transition between the explosive and non-explosive mixtures shows a flame front (Luo et al. 2012), which propagates through fresh mixtures and converts the fresh mixtures to post-ignition mixtures (Shan et al. 2012).

The distributions of Λ_e ($\Lambda_e = sign(\mathrm{Re}(\lambda_e)) \times \log_{10}(\max(1, \mathrm{Re}(\lambda_e)))$) and temperature at different CH_4 concentrations are shown in Figure 10. Owing to the addition of CH_4 in the ambient gas, a clear flame front can be seen between the main flame head and the ambient gas and this flame front is moving downstream with time. After the appearance of the high-temperature reactions triggered by n-heptane, the slow methane oxidation is accelerated. It can be seen from Figure 10b that the area of flame front gets larger, marked as the length of black lines, because the ignition delay is prolonged with a high concentration of CH_4. The spray flame has traveled for a long time at $t^* = 0.6ms$. Therefore, the flame area also gets larger at this time. The combustion of methane outside of the spray plume increases the velocity at the flame surface. It is also shown in Figure 10 that after the ignition of n-heptane spray, the value of Λ_e in the ambient gas is larger than zero and increases with time, indicating that the ambient methane/air mixture becomes explosive. This is due to the temperature increase and compression effects from the combustion of n-heptane spray. Consequently, the unignited methane in the constant volume combustion vessel is quickly consumed, leading to the rapid increase in the mean pressure. In the same time interval relative to the ID, for example at $t^* = 0.6ms$, the value of Λ_e of the surrounding CH_4/air mixture is much greater with high methane concentration in the ambient gas than that with low methane concentration. At higher CH_4 concentration with $\phi_{CH4} = 1.0$, as shown in Figure 10c, Λ_e is very large for all the methane/air mixture in the ambient gas, indicating that auto-ignition for all of the CH_4/air mixture in the ambient gas is on the way. According to Luo et al. (2012), an increase in the equivalence ratio (from 0.5 to 1.0) of the premixed fuel/air mixture can shorten the ignition delay times. For stoichiometric fuel/air mixture, large positive values for λ_e appear very rapidly, which quickly transit to negative values after the high-temperature ignition. In this work, before the arriving of the spray flames, the premixed mixture is auto-ignited due to the temperature increase and compression effects from the reacting spray, especially at 1200 K and $\phi_{CH4} = 1.0$ (not shown here). In addition, it should be noted that different from the results shown in Figure 10a, the spray plume is surrounded by highly explosive mixture at the flame surface with the presence of methane. The combustion regions of dual-fuel/air mixture can be divided into two zones (Liu et al. 2012): the bulk mixture in the inner zone consists of mainly n-heptane, air and methane and the

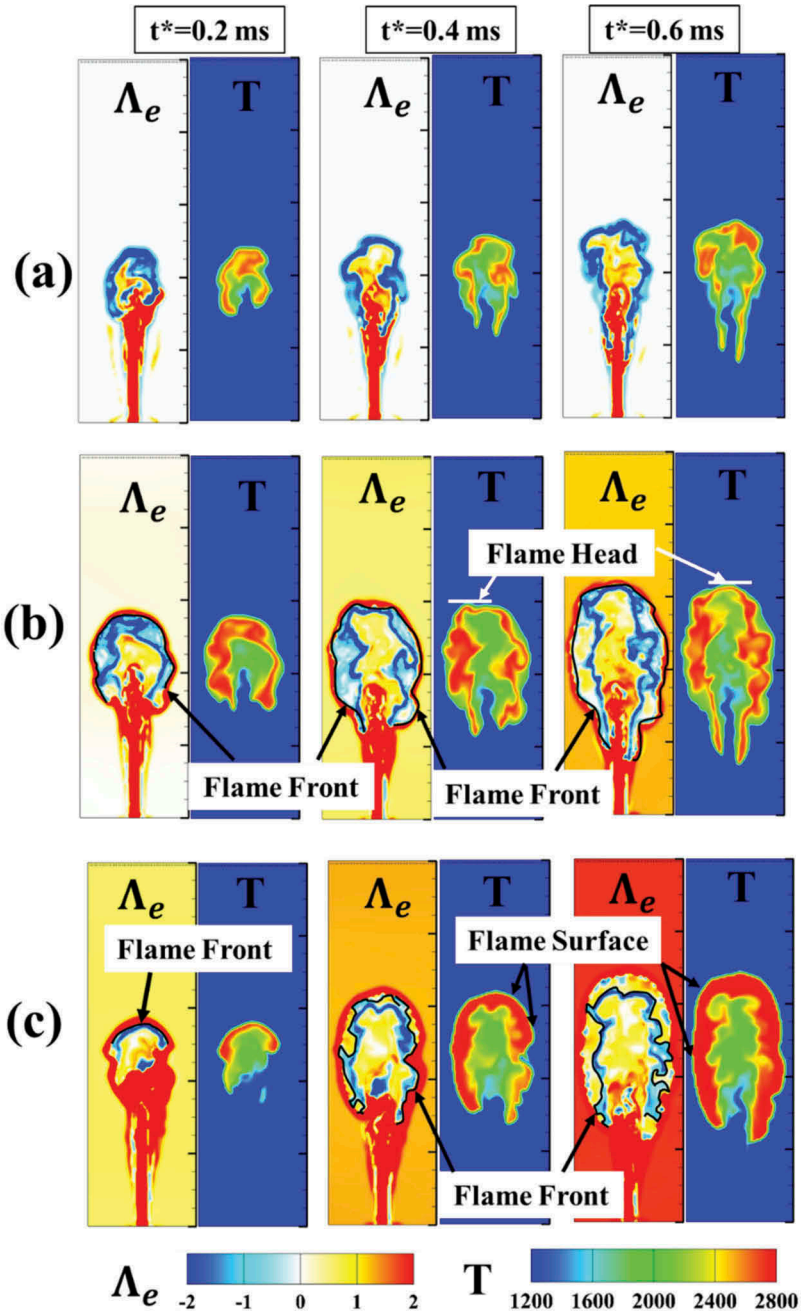

Figure 10. Distinguish between auto-ignition and flame propagation at an initial temperature of 1000 K. (a)$\phi\boxtimes_{CH4} = 0$, (b) $\phi_{CH4} = 0.5$, (c) $\phi_{CH4} = 1.0$. Λ_e is defined as $\Lambda_e = \mathbf{sign}(\mathbf{Re}(\lambda_e)) \times \mathbf{log}_{10}(\mathbf{max}(1, \mathbf{Re}(\lambda_e)))$, where 'sign' represents the sign function, and $\mathbf{Re}(\lambda_e)$ is the real part of the largest non-zero eigenvalue.

other region outside the plume is a diesel-free region consists of air and gaseous methane. Liu et al. (2012) thought that methane/air mixture in the outside region surrounding the n-heptane plume can only be burned by propagating turbulent flames initiated by n-heptane combustion. The two cases shown in Figure 10b,c support the propagation of the turbulent flames. It can be found that adding more methane in the initial gas leads to the increase in the thickness of the outside region of the flame, characterized by large values of Λ_e outside the spray plume. As the combustion of outside combustion region near the flame surface is dominated by the mixing of the hot combustion products and the unburned methane/air mixture (Li et al. 2017), diffusion of the intermediate radical and heat from the n-heptane spray combustion region leads to the explosive mixture there. The highly explosive mixture near the flame front in return accelerates the combustion, and thus, the front moves downstream faster. It is interesting that as shown in Figure 10c at $t^* = 0.6ms$, there are some already burnt regions out of the flame front, characterized by negative values of Λ_e, which is quite different from other figures shown in Figure 10. Since the mixture in the ambient gas is highly explosive, the chemical time scale represented by the reciprocal of λ_e is very small. The overall reaction progress is mainly limited by the local transport and mixing between the highly explosive methane/air mixture and the inner spray plume before the appearance of auto-ignition in the ambient gas.

Flame structures

In order to clearly observe the radial development of flame, temperature and OH contours at the positions of height H = 4 or 5 cm are taken at different times with equivalence ratios of 0.5, and 1.0 in the ambient gas, respectively. As shown in Figure 11, the flame is highly corrugated without CH_4 addition because of the diffusive flame dominating the combustion process. Methane in the ambient gas expands the high-temperature regions along the radial direction, where OH is found in a wider region because when there is no CH_4 in the ambient gas, the radial development of flame is due to the radial velocity component and diffusion. Moreover, the addition of CH_4 accelerates the flame propagation along the radial direction. In the previous studies (Jangi et al. 2013; Pei et al. 2015; Wei et al. 2018c), the decrease in the ignition delay by increasing the oxygen concentrations, gas temperatures, or densities for single fuels leads to thinner flame structures because combustion can prevent the entrainment of fresh air into the spray (Desantes et al. 2014). Consistent with these studies, the prolonged IDs due to the addition of methane in the ambient gas lead to the enhanced entrainment, and thus widening the flame structures. However, it may be caused by another reason. After the appearance of high-temperature reactions, the continually injected fuel pushes the combustion region to the surrounding methane/air mixture. Furthermore, the consumption of methane/air mixture ahead of the spray flames also widens the high-temperature regions. The previous experiments of n-dodecane/air combustion (Srna et al. 2019) have revealed the effect of the ID on the subsequent flame structures, in which Srna et al. compared the CH_2O-PLIF images from a single fuel case and a dual fuel case with similar IDs. Although the temperature of the dual fuel case is much higher, the flame size is quite similar. In addition, the maximum temperature significantly increases at high CH_4 concentration. And the place with maximum

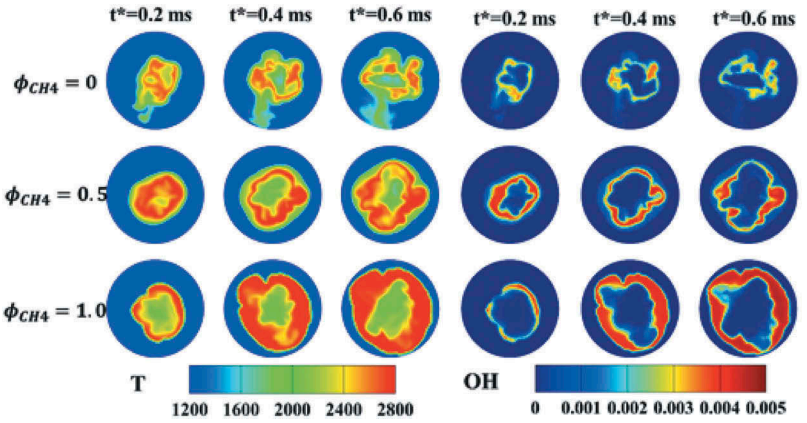

Figure 11. Temperature and OH contours at the place of height = 4 cm for $\phi_{CH4} = 0$, and height = 5 cm for $\phi_{CH4} = 0.5$ and 1.0. The initial temperature is 1000 K.

temperature moves from the inner stoichiometric side to the outer near flame surface side, where more CH_4 is consumed.

To further study the effects of the addition of CH_4 on the development of the flame, Figure 12 shows the position of the axial flame head and flame length at different CH_4 concentrations. The flame head is defined as the farthest position to the injector with the temperature increased by 400 K than that of the initial gas, and the flame length is measured at the farthest and most upstream place with the temperature 400 K higher than the ambient gas. It can be seen from Figure 12 that the flame develops obviously faster at high CH_4 concentration than that without CH_4 addition, which is consistent with the results in Figure 11. The combustion of n-heptane accelerates the spray head moving downstream (Desantes et al. 2014; Payri et al. 2015). Meanwhile, due to the combustion of

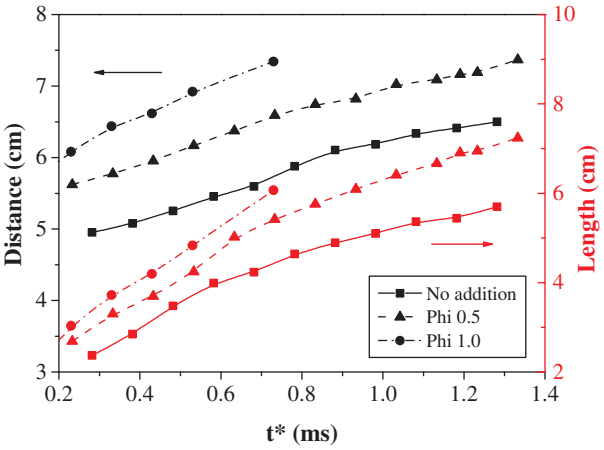

Figure 12. Axial distance and flame length at different CH_4 concentrations at 1000 K.

methane/air mixture at the outside of spray, a diesel-free zone (Liu et al. 2012) further speeds up the spray head. From this respect, it can be concluded that the speed of the flame head consists of two factors: the turbulent spray combustion speed of n-heptane injection involving the flow velocity induced by high-speed injection, and the propagation speed for methane/air mixture at the flame surface. The further downstream flame head location implies that the presence of methane in the background accelerates the movement of the flame head although methane has a smaller laminar flame speed than the large molecular hydrocarbon fuel such as n-dodecane (Ghaderi Masouleh et al. 2017). Furthermore, it can be seen from Figure 12 that by increasing the methane/air equivalence ratio from 0.5 to 1.0, the flame speed for methane/air mixture is increased obviously. Hence, the flame head moves faster to the further downstream locations at a higher methane concentration in the ambient gas.

Conclusions

The ignition characteristics of n-heptane in atmospheres containing methane are numerically investigated using the large eddy simulation coupled with the linear eddy model in a constant-volume combustion vessel. Different levels of CH_4 concentrations in the ambient gas are adopted. By increasing the CH_4 mole fraction in the initial environment, the ignition delay time (ID) is prolonged significantly at a low initial temperature. However, slight differences in the ID can be seen at high temperatures. The addition of CH_4 leads to a longer first-stage ignition process at a low initial temperature. By adding more CH_4 in the ambient gas, the mixture firstly auto-ignited becomes much fuel-richer, which is independent of the initial ambient gas temperature. According to the chemical explosive mode analysis (CEMA) method, the development of flame structures is significantly influenced by the addition of CH_4. No explosive mixture exists in the flame head regions without any CH_4 in the ambient gas. A transition between the explosive and non-explosive mixtures is observed by the addition of CH_4, indicating that a flame front appears at the flame head and develops further downstream. The eigenvalue of the Jacobian matrix for the unburnt methane/air mixture increases quickly at high CH_4 concentration, implying that methane/air is ready to autoignite because of the temperature increase and compression effects from the combustion of n-heptane spray flames. Finally, the analysis on the development of flame structures shows that at higher CH_4 concentration, the flame surface develops more quickly due to the better fuel/air mixing caused by the longer ignition delay, and the most intense combustion regions with the maximum temperature moves from the inner side to the outer side.

Disclosure statement

We declare that we have no conflict of interest.

Funding

The work is supported by National Natural Science Foundation of China (Grant No. 91741119, 51606133, 91641203) and Marine Low-Speed Engine Project (Phase I). The work was carried out at National Supercomputer Center in Tianjin, and the calculations were performed on TianHe-1 (A).

References

Agarwal, A. K., A. P. Singh, and R. K. Maurya. 2017. Evolution, challenges and path forward for low temperature combustion engines. *Prog. Energy Combust. Sci.* 61:1–56. doi:10.1016/j.pecs.2017.02.001.

Aggarwal, S. K., O. Awomolo, and K. Akber. 2011. Ignition characteristics of heptane–hydrogen and heptane–methane fuel blends at elevated pressures. *Int. J. Hydrogen Energy* 36:15392–402. doi:10.1016/j.ijhydene.2011.08.065.

Amsden, A. A. 1997. *KIVA3V: a block-structured KIVA program for engines with vertical or canted valves*. Los Alamos: Los Alamos National Lab.

Azimov, U., K.-S. Kim, and C. Bae. 2010. Modeling of flame lift-off length in diesel low-temperature combustion with multi-dimensional CFD based on the flame surface density and extinction concept. *Combust. Theory Modell.* 14:155–75. doi:10.1080/13647831003713930.

Bekdemir, C., L. M. T. Somers, L. P. H. de Goey, J. Tillou, and C. Angelberger. 2013. Predicting diesel combustion characteristics with large-eddy simulations including tabulated chemical kinetics. *Proc. Combust. Inst.* 34:3067–74. doi:10.1016/j.proci.2012.06.160.

Bharadwaj, N., C. Rutland, and S. Chang. 2009. Large eddy simulation modelling of spray-induced turbulence effects. *Int. J. Engine Res.* 10:97–119. doi:10.1243/14680874JER02309.

CHEMKIN-PRO 15131. 2013. *Reaction design*. CA: San Diego.

Daca, A. E., and Ö. L. Gülder. 2017. Soot formation characteristics of diffusion flames of methane doped with toluene and n-heptane at elevated pressures. *Proc. Combust. Inst.* 36:737–44. doi:10.1016/j.proci.2016.07.046.

Demosthenous, E., G. Borghesi, E. Mastorakos, and R. S. Cant. 2016. Direct numerical simulations of premixed methane flame initiation by pilot n-heptane spray autoignition. *Combust. Flame* 163:122–37. doi:10.1016/j.combustflame.2015.09.013.

Desantes, J. M., J. V. Pastor, J. M. García-Oliver, and F. J. Briceño. 2014. An experimental analysis on the evolution of the transient tip penetration in reacting diesel sprays. *Combust. Flame* 161:2137–50. doi:10.1016/j.combustflame.2014.01.022.

Fu, J., J. Shu, F. Zhou, J. Liu, Z. Xu, and D. Zeng. 2017. Experimental investigation on the effects of compression ratio on in-cylinder combustion process and performance improvement of liquefied methane engine. *Appl. Therm. Eng.* 113:1208–18. doi:10.1016/j.applthermaleng.2016.11.048.

García-Oliver, J. M., L.-M. Malbec, H. B. Toda, and G. Bruneaux. 2017. A study on the interaction between local flow and flame structure for mixing-controlled diesel sprays. *Combust. Flame* 179:157–71. doi:10.1016/j.combustflame.2017.01.023.

Ghaderi Masouleh, M., A. Wehrfritz, O. Kaario, H. Kahila, and V. Vuorinen. 2017. Comparative study on chemical kinetic schemes for dual-fuel combustion of n-dodecane/methane blends. *Fuel* 191:62–76. doi:10.1016/j.fuel.2016.10.114.

Idicheria, C. A., and L. M. Pickett. 2007. Quantitative mixing measurements in a vaporizing diesel spray by Rayleigh imaging. SAE Technical Paper, No. 2007-01-0647. doi:10.1094/PDIS-91-4-0467B.

Irannejad, A., A. Banaeizadeh, and F. Jaberi. 2015. Large eddy simulation of turbulent spray combustion. *Combust. Flame* 162:431–50. doi:10.1016/j.combustflame.2014.07.029.

Jangi, M., T. Lucchini, G. D'Errico, and X.-S. Bai. 2013. Effects of EGR on the structure and emissions of diesel combustion. *Proc. Combust. Inst.* 34:3091–98. doi:10.1016/j.proci.2012.06.093.

Karim, G. A. 2003. Combustion in gas fueled compression: Ignition engines of the dual fuel type. *J. Eng. Gas Turbines Power* 125:827–36. doi:10.1115/1.1581894.

Kerstein, A. R. 1989. Linear-eddy modeling of turbulent transport. II: Application to shear layer mixing. *Combust. Flame* 75:397–413. doi:10.1016/0010-2180(89)90051-5.

Kundu, P., M. M. Ameen, and S. Som. 2017. Importance of turbulence-chemistry interactions at low temperature engine conditions. *Combust. Flame* 183:283–98. doi:10.1016/j.combustflame.2017.05.025.

Levine, R. D. 2009. *Molecular reaction dynamics*. UK: Cambridge University Press.

Li, Y., H. Li, H. Guo, Y. Li, and M. Yao. 2017. A numerical investigation on methane combustion and emissions from a natural gas-diesel dual fuel engine using CFD model. *Appl. Energy* 205:153–62. doi:10.1016/j.apenergy.2017.07.071.

Liu, S., H. Li, T. Gatts, C. Liew, S. Wayne, G. Thompson, N. Clark, and J. Nuszkowski. 2012. An investigation of NO2 emissions from a heavy-duty diesel engine fumigated with H2 and natural gas. *Combust. Sci. Technol.* 184:2008–35. doi:10.1080/00102202.2012.695828.

Liu, S. L., J. C. Hewson, J. H. Chen, and H. Pitsch. 2004. Effects of strain rate on high-pressure nonpremixed n-heptane autoignition in counterflow. *Combust. Flame* 137:320–39. doi:10.1016/j.combustflame.2004.01.011.

Luo, Z., C. S. Yoo, E. S. Richardson, J. H. Chen, C. K. Law, and T. Lu. 2012. Chemical explosive mode analysis for a turbulent lifted ethylene jet flame in highly-heated coflow. *Combust. Flame* 159:265–74. doi:10.1016/j.combustflame.2011.05.023.

Manias, D. M., E. A. Tingas, C. E. Frouzakis, K. Boulouchos, and D. A. Goussis. 2016. The mechanism by which CH2O and H2O2 additives affect the autoignition of CH4/air mixtures. *Combust. Flame* 164:111–25. doi:10.1016/j.combustflame.2015.11.008.

Martinez, D. M., X. Jiang, C. Moulinec, and D. Emerson. 2014. Numerical assessment of subgrid scale models for scalar transport in large-eddy simulations of hydrogen-enriched fuels. *Int. J. Hydrogen Energy* 39:7173–89. doi:10.1016/j.ijhydene.2014.03.018.

Mastorakos, E. 2009. Ignition of turbulent non-premixed flames. *Prog. Energy Combust. Sci.* 35:57–97. doi:10.1016/j.pecs.2008.07.002.

O'Rourke, P. J. 1981. collective drop effects on vaporizing liquid sprays. *Engineering.* New Mexico, US: ALos Alamos National Lab.

Papagiannakis, R. G., and D. T. Hountalas. 2004. Combustion and exhaust emission characteristics of a dual fuel compression ignition engine operated with pilot diesel fuel and natural gas. *Energy Convers. Manage.* 45:2971–87. doi:10.1016/j.enconman.2004.01.013.

Patterson, M. A., and R. D. Reitz. 1998. *Modeling the effects of fuel spray characteristics on diesel engine combustion and emission*. Detroit, USA: SAE International.

Payri, R., J. M. García-Oliver, T. Xuan, and M. Bardi. 2015. A study on diesel spray tip penetration and radial expansion under reacting conditions. *Appl. Therm. Eng.* 90:619–29. doi:10.1016/j.applthermaleng.2015.07.042.

Pei, Y., E. R. Hawkes, M. Bolla, S. Kook, G. M. Goldin, Y. Yang, S. B. Pope, and S. Som. 2016. An analysis of the structure of an n-dodecane spray flame using TPDF modelling. *Combust. Flame* 168:420–35. doi:10.1016/j.combustflame.2015.11.034.

Pei, Y., S. Som, E. Pomraning, P. K. Senecal, S. A. Skeen, J. Manin, and L. M. Pickett. 2015. Large eddy simulation of a reacting spray flame with multiple realizations under compression ignition engine conditions. *Combust. Flame* 162:4442–55. doi:10.1016/j.combustflame.2015.08.010.

Pickett, L. M. 2019. Engine combustion network. http://www.sandia.gov/ecn/

Pickett, L. M., and D. L. Siebers. 2004. Soot in diesel fuel jets: effects of ambient temperature, ambient density, and injection pressure. *Combust. Flame* 138:114–35. doi:10.1016/j.combustflame.2004.04.006.

Schlatter, S., B. Schneider, Y. Wright, and K. Boulouchos. 2012. Experimental study of ignition and combustion characteristics of a diesel pilot spray in a lean premixed methane/air charge using a rapid compression expansion machine. SAE 2012 World Congress and Exhibition, Detroit, MI: SAE International, April 24–26. doi:10.1094/PDIS-11-11-0999-PDN.

Schlatter, S., B. Schneider, Y. M. Wright, and K. Boulouchos. 2016. N-heptane micro pilot assisted methane combustion in a rapid compression expansion machine. *Fuel* 179:339–52. doi:10.1016/j.fuel.2016.03.006.

Shan, R., C. S. Yoo, J. H. Chen, and T. Lu. 2012. Computational diagnostics for n-heptane flames with chemical explosive mode analysis. *Combust. Flame* 159:3119–27. doi:10.1016/j.combustflame.2012.05.012.

Smith, G. P. G., M. David, M. Frenklach, N. W. Moriarty, B. Eiteneer, M. Goldenberg, T. Bowman, R. K. Hanson, S. Song, W. C. Gardiner, et al. http://www.me.berkeley.edu/gri_mech/.

Sone, K., N. Patel, and S. Menon. 2001.Large-eddy simulation of fuel-air mixing in an internal combustion engine. 39th Aerospace Sciences Meeting and Exhibit, Reno, NV, 635.

Sone, K., and S. Menon. 2003. Effect of subgrid modeling on the in-cylinder unsteady mixing process in a direct injection engine. *J. Eng. Gas Turbines Power* 125:435–43. doi:10.1115/1.1501918.

Soriano, B. S., E. S. Richardson, S. Schlatter, and Y. M. Wright. 2017. *Conditional moment closure modelling for dual-fuel combustion engines with pilot-assisted compression ignition*. Detroit, USA: SAE International.

Srna, A., M. Bolla, Y. M. Wright, K. Herrmann, R. Bombach, S. S. Pandurangi, K. Boulouchos, and G. Bruneaux. 2019. Effect of methane on pilot-fuel auto-ignition in dual-fuel engines. *Proc. Combust. Inst* 37: 4741–4749.

van Leer, B. 1974. Towards the ultimate conservative difference scheme. II. Monotonicity and conservation combined in a second-order scheme. *J Comput Phys* 14:361–70. doi:10.1016/0021-9991(74)90019-9.

Wang, Z., and J. Abraham. 2015. Fundamental physics of flame development in an autoigniting dual fuel mixture. *Proc. Combust. Inst.* 35:1041–48. doi:10.1016/j.proci.2014.06.079.

Wei, H., J. Qi, L. Zhou, W. Zhao, and G. Shu. 2018a. Ignition characteristics of methane/n-heptane fuel blends under engine-like conditions. *Energy Fuels* 32:6264–77. doi:10.1021/acs.energyfuels.7b04128.

Wei, H., W. Zhao, L. Zhou, C. Chen, and G. Shu. 2018b. Large eddy simulation of the low temperature ignition and combustion processes on spray flame with the linear eddy model. *Combust. Theory Modell.* 22:237–63. doi:10.1080/13647830.2017.1392044.

Wei, H., W. Zhao, L. Zhou, and G. Shu. 2018c. Numerical investigation of diesel spray flame structures under diesel engine-relevant conditions using large eddy simulation. *Combust. Sci. Technol.* 190:909–32. doi:10.1080/00102202.2017.1417270.

Wei, H., W. Zhao, Z. Lu, and L. Zhou. 2019. Effects of oxygen concentrations on the ignition and quasi-steady processes of n-heptane spray flames using large eddy simulation. *Fuel* 241:786–801. doi:10.1016/j.fuel.2018.12.097.

Wu, Z., C. J. Rutland, and Z. Han. 2019. Numerical evaluation of the effect of methane number on natural gas and diesel dual-fuel combustion. *Int. J. Engine Res.* 1468087418758114.

Yao, M., Z. Zheng, and H. Liu. 2009. Progress and recent trends in homogeneous charge compression ignition (HCCI) engines. *Prog. Energy Combust. Sci.* 35:398–437. doi:10.1016/j.pecs.2009.05.001.

Yousefi, A., M. Birouk, and H. Guo. 2017a. An experimental and numerical study of the effect of diesel injection timing on natural gas/diesel dual-fuel combustion at low load. *Fuel* 203:642–57. doi:10.1016/j.fuel.2017.05.009.

Yousefi, A., M. Birouk, and H. Guo. 2017b. An experimental and numerical study of the effect of diesel injection timing on natural gas/diesel dual-fuel combustion at low load. *Fuel* 203:642–57. doi:10.1016/j.fuel.2017.05.009.

Zhang, P., J. Ran, C. Qin, X. Du, J. Niu, and L. Yang. 2018. Effects of methane addition on exhaust gas emissions and combustion efficiency of the premixed n-heptane/Air combustion. *Energy Fuels* 32:3900–07. doi:10.1021/acs.energyfuels.7b03469.

Zhang, P., W. Ji, T. He, X. He, Z. Wang, B. Yang, and C. K. Law. 2016. First-stage ignition delay in the negative temperature coefficient behavior: Experiment and simulation. *Combust. Flame* 167:14–23. doi:10.1016/j.combustflame.2016.03.002.

Zhou, L., K. H. Luo, W. Qin, M. Jia, and S. J. Shuai. 2015. Large eddy simulation of spray and combustion characteristics with realistic chemistry and high-order numerical scheme under diesel engine-like conditions. *Energy Convers. Manage.* 93:377–87. doi:10.1016/j.enconman.2015.01.033.

Zhou, L., M. Xie, M. Jia, Q. Zhou, and C. Xu. 2011. *Influences of subgrid turbulent kinetic energy and turbulent dispersion on the characteristics of fuel spray*. Detroit, USA: SAE International.

Zhou, L., W. Zhao, and H. Wei. 2018. Large eddy simulation on the flame structure for split injections of n-dodecane at different temperatures and densities. *Combust. Sci. Technol.* 190:2224–44. doi:10.1080/00102202.2018.1498485.